ACS Energy LETTERS

http://pubs.acs.org/journal/aelccp

# Pliable Lithium Superionic Conductor for All-Solid-State Batteries

Sung-Kyun Jung,*,§ Hyeokjo Gwon,*,§ Gabin Yoon, Lincoln J. Miara, Valentina Lacivita, and Ju-Sik Kim

Cite This: *ACS Energy Lett.* 2021, 6, 2006−2015

Read Online

ACCESS | Metrics & More | Article Recommendations | Supporting Information

**ABSTRACT:** The key challenges in all-solid-state batteries (ASSBs) are establishing and maintaining perfect physical contact between rigid components for facile interfacial charge transfer, particularly between the solid electrolyte and cathode, during repeated electrochemical cycling. Here, we introduce inorganic-based pliable solid electrolytes that exhibit extraordinary clay-like mechanical properties (storage and loss moduli <1 MPa) at room temperature, high lithium-ion conductivity (3.6 mS $cm^{-1}$), and a glass transition below −50 °C. The unique mechanical features enabled the solid electrolyte to penetrate into the high-loading cathode like liquid, thereby providing complete ionic conduction paths for all cathode particles as well as maintaining the pathway even during cell operation. We propose a design principle in which the complex anion formation including Ga, F, and a different halogen can induce the clay-like features. Our findings provide new opportunities in the search for solid electrolytes and suggest a new approach for resolving the issues caused by the solid electrolyte−cathode interface in ASSBs.

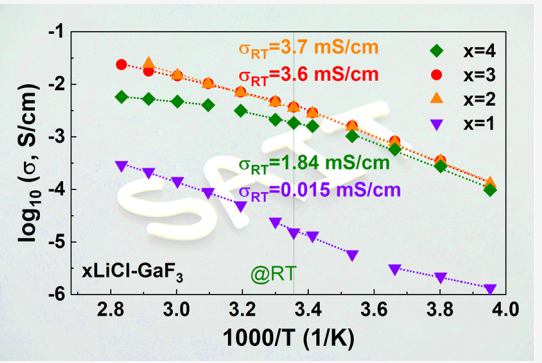


The field of battery research is in the midst of a paradigm shift from conventional liquid electrolyte systems to all-solid-state batteries (ASSBs) owing to their high safety and potentially large volumetric energy density by enabling both the use of lithium metal anodes and the bipolar stacking of electrodes.[1,2] This transition brings a significant change in the kinetics of interfacial electrochemistry governing the battery performance because of the rigid solid−solid interface in ASSBs.[3−6] In a typical liquid electrolyte cell, the active material surface is completely covered by the fluidic electrolyte, whereas a solid electrolyte forms a point contact with the active material owing to its intrinsically rigid nature, thereby inducing sluggish charge transfer and mass transport kinetics at the interface.

Thus, to achieve ASSBs, an important prerequisite is forming and maintaining a well-defined solid−solid interface with intimate contact between the solid electrolytes and cathode/anode active materials during electrochemical cycling. The anode−solid electrolyte interface, represented by a metal−ceramic interface, maintains intimate contact relatively easily, regardless of the type of electrolyte, owing to the ductile nature of lithium metal. In addition, alloying with other metals or incorporating interlayers facilitates the maintenance of intimate contact with the solid electrolyte by keeping the interfacial resistance low during electrochemical cycling.[7,8] Meanwhile, because cathodes have a random porous structure, forming a well-defined cathode−electrolyte interface fully covered by a solid electrolyte is difficult, which can result in inhomogeneous electronic and ionic conduction in the cathode. Further, this interface is a rigid ceramic−ceramic contact, making it more challenging to establish and maintain intimate contact.

Current solid electrolyte systems that are considered promising candidates in terms of lithium-ion conductivity (e.g., garnet, argyrodite, halide, and hydride)[9−12] require additional engineering for intimate cathode−electrolyte contact, such as cosintering,[13,14] maintaining external pressure,[15] or adding an ionic liquid.[16] However, cosintering can cause thermal decomposition or chemical diffusion[17,18] and incorporating a device to apply pressure can occupy considerable space, thus decreasing the volumetric energy density. In particular, because these materials are in the class of inorganic solids, their deformability is limited, which makes it challenging to maintain close contact at the solid−solid interface. Meanwhile, solid polymer electrolytes satisfy the requirements of deformability, but their low ionic conductivity[19] and safety concern regarding thermal vulnerability

**Received:** March 14, 2021
**Accepted:** April 29, 2021
**Published:** May 4, 2021

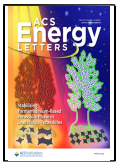







https://doi.org/10.1021/acsenergylett.1c00545
*ACS Energy Lett.* 2021, 6, 2006−2015

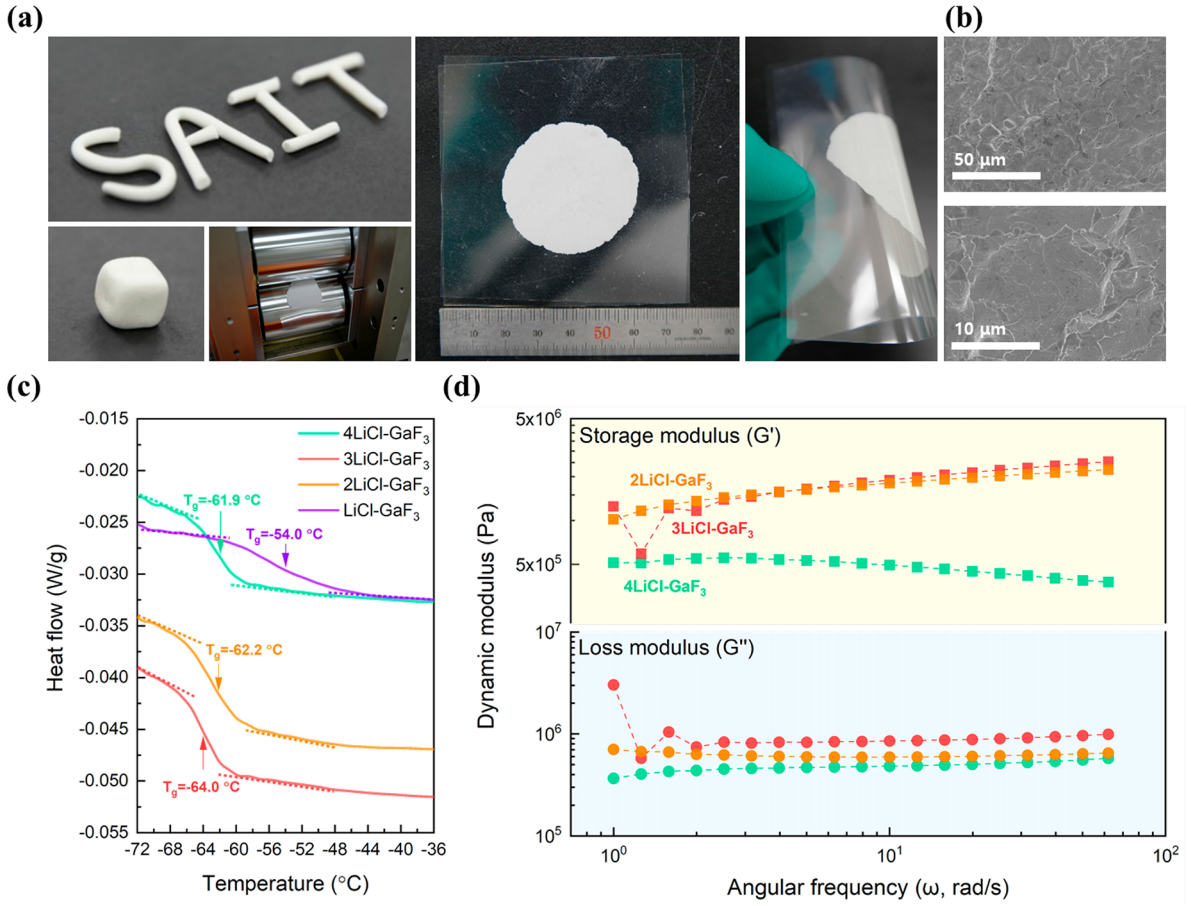


**Figure 1. Pliable characteristics of $x$LiCl−$GaF_3$ ($1 \leq x \leq 4$) composite. (a) Optical images confirming the room-temperature formability of the 2LiCl−$GaF_3$ composite. (b) SEM images of the 2LiCl−$GaF_3$ composite. (c) DSC curves exhibiting glass transitions under −60 °C. (d) Rheological properties of the $x$LiCl−$GaF_3$ ($1 \leq x \leq 4$) composite.**

remain critical issues. Solid-type hybrid electrolytes represented by polymer−ionic liquid−inorganic compounds (e.g., solid−liquid composite electrolytes) have been suggested as an alternative for overcoming this low ionic conductivity; however, the ionic conductivity of the majority of compounds remains within $10^{-4}$ S/cm, because the amount of ionic liquid is limited to form a self-supporting membrane.[20,21] In addition, cathode electrodes with low loading densities of cathode active materials (below 3 mg $cm^{-2}$) have been primarily applied for evaluation. In contrast, the feasibility of these electrolytes in thick and porous cathode electrodes with high loading densities (over 10 mg $cm^{-2}$) have yet to be evaluated, perhaps due to the potentially veiled issue on the application of high-loading-density cathode electrodes.[22]

Due to these limitations, i.e., the unsuitable mechanical properties of inorganic solid electrolytes and the poor chemical properties of polymer electrolytes, it is of interest to design a new class of freely deformable, inorganic-based electrolytes. Here, we report a pliable solid electrolyte combining the advantages of both polymer and inorganic materials, i.e., clay-like rheological properties (storage and loss moduli <1 MPa) with a low glass transition temperature (−60 °C) and high ionic conductivity (3.6 mS $cm^{-1}$). Complex anion formation with Ga, F, and a different halogen is critical to achieve both clay-like viscoelasticity and high ionic conductivity. Owing to its soft physical properties, this electrolyte can function as a catholyte for ASSBs by forming and maintaining intimate contact with a commercial lithium nickel cobalt manganese oxide (NCM) electrode with a high loading density (~20 mg $cm^{-2}$).

*Synthesis of material and rheological character*. Pliable solid electrolytes were mechanochemically prepared by mixing as-received LiCl and $GaF_3$ precursors ($x$LiCl−$GaF_3$, $1 \leq x \leq 4$) (Figure S1). The composition is similar to the recently reported halide-based $Li_3MX_6$ (M = Y, In, Sc, Er, etc./X = F, Cl, Br, I) electrolytes;[11,23−27] however, it is acquired as a glass-like amorphous phase. By varying the mixing ratio of LiCl and $GaF_3$, an approximately pure phase was obtained at the composition of $x$ = 2, with the formation of chemical bonds with $F^-$ or $Cl^-$ bound to Ga (Figure S2) accompanied by a local structural evolution forming four-coordination geometry (Figure S3), which is often observed in gallium-containing, static, disordered phases.[28,29]

The pliable electrolytes show unique clay-like physical properties, exhibiting rheological behavior with high plasticity at room temperature (Figure 1(a)), which means that their shape is readily transformed by kneading (Video S1). In addition, we can easily control their thickness by a roll-to-roll process, and they even show flexibility without crack formation when bent. Scanning electron microscopy (SEM) images of 2LiCl−$GaF_3$ reveal a compact morphology without grain boundaries, similar to that of a glassy matrix (Figure 1(b)), which is commonly observed in glass and cold-pressed glass−ceramic electrolytes.[30] Differential scanning calorimetry (DSC) curves (Figure 1(c)) exhibit glass transition behavior (glass transition temperature, $T_g \approx -60$ °C), explaining their


https://doi.org/10.1021/acsenergylett.1c00545
ACS Energy Lett. 2021, 6, 2006−2015

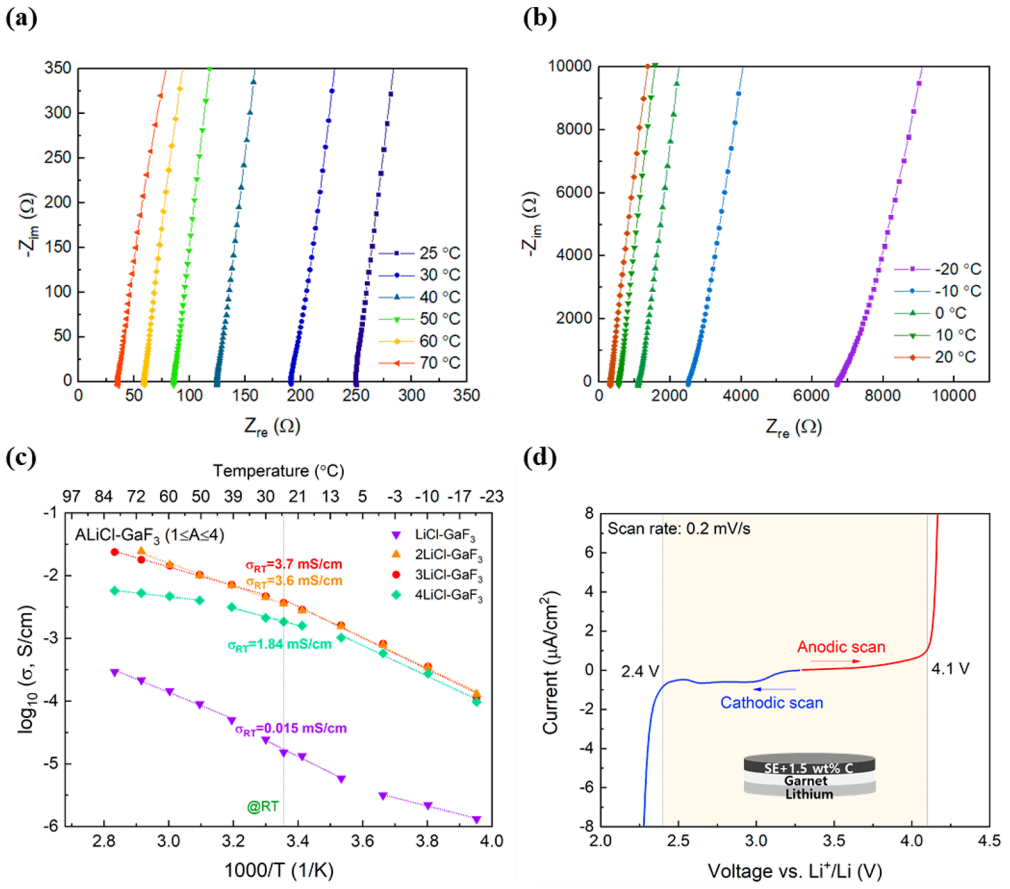


**Figure 2. Ionic conductivity and stability of $x$LiCl−$GaF_3$ ($1 \le x \le 4$) composite solid electrolytes. (a,b) Impedance spectra of 2LiCl−$GaF_3$ electrolytes with 4940 $\mu$m thickness and 0.567 $cm^2$ electrode area in the SUS/2LiCl−$GaF_3$/SUS configuration at various temperatures. (c) Arrhenius plots of the bulk conductivity of $x$LiCl−$GaF_3$ ($1 \le x \le 4$) composite electrolytes. (d) Cyclic voltammetry (CV) and electrochemical stability window (shaded area) of Li/LLZTO/2LiCl−$GaF_3$ with a 1.5 wt % carbon/SUS cell at a scan rate of 0.2 mV $s^{-1}$.**

clay-like state at room temperature. This $T_g$ is lower than those of supramolecular lithium-ion conductors (−49 °C), polymers (−29 °C),[31] and glass-type solid electrolytes (128−210 °C).[32,33] The rheological properties of the solid electrolytes were quantified using a rheometer, and the storage ($G'$) and loss ($G''$) moduli were plotted as a function of frequency (Figure 1(d)). All moduli were in the range of $10^5$−$10^6$ Pa and exhibited a phase shift of less than 45°, indicating clay-like solid properties. In addition, the complex, shear moduli were on the same order of magnitude as that of a viscoelastic, gum-like, polymer electrolyte of $0.2 \times 10^6$ Pa.[34]

*Lithium superionic conductor as solid electrolyte.* We also measured the lithium-ion conductivity and electrochemical stability window of xLiCl−$GaF_3$ to evaluate its feasibility as a solid electrolyte. The ionic conductivity was measured by potentiostatic electrochemical impedance spectroscopy (PEIS) from −20−80 °C with a cell configuration of stainless steel (SS)/solid electrolyte (SE)/SS and no additional external pressure. As shown in Figure 2(a), 2LiCl−$GaF_3$ showed bulk resistance under 250 Ω at and above 25 °C, and even at low temperatures (−20 °C, Figure 2(b)), only the bulk resistance was shown with no grain boundary resistance. Given that the bulk resistance of solid electrolytes is on the order of tens of ohms over 30 °C, we subtracted the cable impedance (a few ohms) to acquire the exact value of ionic conductivity (Table S1). In the Arrhenius plots of bulk ionic conductivity for various compositions of xLiCl−$GaF_3$ ($1 \le x \le 4$) in Figure 2(c), 2LiCl−$GaF_3$ and 3LiCl−$GaF_3$ showed the highest values of ionic conductivity of 3.6−3.7 mS $cm^{-1}$ at room temperature, and its DC electronic conductivity was estimated to be $4-5 \times 10^{-9}$ S $cm^{-1}$ (Figure S4). The activation energy of 2LiCl−$GaF_3$ was 364.3 meV at and above room temperature (25 °C) but increased to 490 meV below 25 °C. As the amount of LiCl increased to $x$ = 4, the room-temperature ionic conductivity decreased to 1.84 mS $cm^{-1}$ (Figure S5), which may have been due to the excess LiCl that did not form anion complexes observed in X-ray diffraction (XRD), which had a low ionic conductivity (~$10^{-6}$ S $cm^{-1}$). Conversely, the lowest ionic conductivity of 0.015 mS $cm^{-1}$ at $x$ = 1 was due to the insufficient amount of LiCl for forming the ion-conducting phase. Non-Arrhenius, temperature-dependent, ionic conductivity, which is shown in glass or polymer electrolytes above the glass transition temperature,[35] may be due to the coupling behavior of ionic transport with sliding or translation of the structural network similar to the motion of polymer chains in the polymer electrolyte. Given that the glass transition temperature was far below room temperature and the rheological behavior, the temperature-dependent viscosity change of the $x$LiCl−$GaF_3$ solid electrolyte could be responsible for the non-Arrhenius relationship of ionic conductivity as a function of temperature. This implied that the high ionic conductivity of xLiCl−$GaF_3$ originated from the fluidic behavior. In fact, the solid electrolyte with


https://doi.org/10.1021/acsenergylett.1c00545
ACS Energy Lett. 2021, 6, 2006−2015

clay-like features showed high ionic conductivity compared to the powder state (Table 1).

**Table 1. Rheological Behavior and Ionic Conductivity of Solid Electrolytes with Various Combinations**

| composition | main cation | main anion | different halogen | physical state | ionic conductivity (@ RT, mS $cm^{-1}$) |
|---|---|---|---|---|---|
| $2LiCl-GaF_3$ | Ga | F | Cl | clay-like | 3.6 |
| $3LiCl-GaF_3$ | Ga | F | Cl | clay-like | 3.7 |
| $4LiCl-GaF_3$ | Ga | F | Cl | clay-like | 1.84 |
| $3LiBr-GaF_3$ | Ga | F | Br | clay-like | 0.43 |
| $2LiCl-LiOH-GaF_3$ | Ga | F | Cl | clay-like | 2.0 |
| $3LiCl-0.1LaCl_3-0.9GaF_3$ | Ga | F | Cl | clay-like | 1.34 |
| $3LiCl-0.1InCl_3-0.9GaF_3$ | Ga | F | Cl | clay-like | 2.32 |
| $3LiOH-GaF_3$ | Ga | F | - | powder | 0.17 |
| $Li_2O-GaF_3$ | Ga | F | - | powder | too low to measure |
| $3LiCl-LaF_3$ | La | F | Cl | powder | too low to measure |
| $3LiCl-InF_3$ | In | F | Cl | powder | too low to measure |
| $6LiCl-Ga_2O_3$ | Ga | O | - | powder | too low to measure |
| $3LiCl-GaCl_3$ | Ga | Cl | - | powder | $1.57 \times 10^{-2}$ |
| $LiCl-GaCl_3$ | Ga | Cl | - | powder | $7.48 \times 10^{-3}$ |

Cyclic voltammetry (CV) was performed to measure the electrochemical stability of the $2LiCl-GaF_3$ compounds, which exhibited the highest ionic conductivity (Figure 2(d)). The cell was configured as Li/garnet/SE + carbon. Carbon was added to the solid electrolyte given the recent report that the electrochemical stability depends on the decomposition pathway of the (de)lithiated state of a solid electrolyte.[36] Garnet ($Li_{6.5}La_3Zr_{1.5}Ta_{0.5}O_{12}$, LLZTO) was applied, because $2LiCl-GaF_3$ is unstable in contact with Li metal (Figure S6). The anodic and cathodic voltage scans at 0.2 mV $s^{-1}$ both began at the open-circuit potential of 3.28 V and revealed reaction peaks at 4.1 and 2.4 V versus the reduction potential of lithium, respectively. Since the anodic stability of materials is primarily determined by the dissociation of Li binary phases, a relatively high anodic stability, in agreement with other Cl-based materials, was observed for $2LiCl-GaF_3$.[37] On the other hand, the cathodic limit was relatively high compared to other recently reported halides, presumably due to the vulnerability of $Ga^{3+}$ against reduction. To compare the reduction stabilities of various metal species in halide solid electrolytes, we calculated their thermodynamic electrochemical stabilities by performing density functional theory (DFT) calculations for recently reported halides (with a composition of $Li_3MX_6$) and Ga-substituted versions. The Ga-substituted versions possessed a different crystal structure from $xLiCl-GaF_3$; however, calculations using isostructural models enabled us to directly compare the effect of metal species on the reductive stability, isolated from the other possible factors, such as structural effects. The reduction stability was indeed dependent on the metal species (Table S2), and $Ga^{3+}$ was readily reduced to $Ga^{2+}$ or $Ga^0$ above 2 V regardless of the anion species, while $Y^{3+}$ and $Sc^{3+}$ were not reduced until ~0.9 V.

Stability in the presence of ambient air and water was investigated in addition to the electrochemical stability. Owing to their hygroscopicity, the clay-like solid electrolytes turned into gels with low viscosity after exposure to ambient air for 24 h. Adding 10−30 wt % of water to the $xLiCl-GaF_3$ solid electrolytes increased their ionic conductivity to over 10 mS $cm^{-1}$ at room temperature (Figure S7), whereas humid air usually decreases the ionic conductivity of sulfide and halide electrolytes.[23] This increase may be due to the formation of $LiCl{\cdot}xH_2O$, which has a high ionic conductivity (more than 10 mS $cm^{-1}$).[38]

*Ga-containing complex anions for clay-like solid electrolytes.* Inspired by the chemical tunability of the pliable electrolyte observed while varying the composition ($xLiCl-GaF_3$, $1 \leq x \leq 4$), we also explored the chemical space showing both rheological properties and high ionic conductivity. LiBr and LiOH were separately applied as lithium sources for mechanochemical mixing with $GaF_3$. Both $3LiBr-GaF_3$ and $3LiOH-GaF_3$ showed ionic conductivities of 0.43 and 0.17 mS $cm^{-1}$ at room temperature, respectively (Figure S8). $3LiBr-GaF_3$ showed clay-like rheological behavior with a low $T_g$ (−57.6 °C, Figure S9), unlike $3LiOH-GaF_3$, which remained in the powder state. Notably, adding different kinds of halogen atoms other than the gallium and fluorine further benefitted the rheological behavior and high ionic conductivity (Table 1).

In particular, the rheological behavior is thought to originate in the formation of complex anions in an amorphous matrix, which is different from the mechanism underlying the clay-like properties of other electrolyte materials, which are imparted by water. In those electrolytes, compounds form such as $Li_{3-x}H_xOCl$ or hydrated lithium hydroxide $LiCl{\cdot}xH_2O$,[33,38] which show a lower activation energy (80−140 meV). These low activation energies were presumed to be similar to the solvent-mediated ion transport that demonstrated a value of approximately 80−160 meV.[39] However, $xLiCl-GaF_3$ ($x$ = 2, 3) solid electrolytes showed higher activation energies in the range of 300−500 meV, which indicated that the ion transport mechanism was different from water-mediated ion transport. In contrast, a drastic decrease in activation energy from 513 to 188 meV was observed when we intentionally added 10 wt % of deionized (DI) water to the $3LiCl-GaF_3$ solid electrolyte (Figure S10). In addition, considering that the water content requirement of glass-forming for LiCl is between 63 and 77 wt %,[40] the water content in our system was too low to impart viscoelasticity (Figure S11). All of the absorbed residual water in the $xLiCl-GaF_3$ electrolyte was released in the form of $H_2O$ or HCl at temperatures below 200 °C, and there was no structural water released at temperatures above 200 °C, from the evolved gas analysis (EGA) measurements (Figure S12). Therefore, the effect of the water content in the $xLiCl-GaF_3$ solid electrolyte on both its rheological properties and fast ion conduction was insignificant. Instead, the glass-forming ability, which was correlated with the glass transition temperature, was affected by the formation of complex anions in the compounds.

In gallium-containing chalcohalide glasses, adding a halogen or halide increases the glass-forming ability. For example, incorporating a metal chloride into the $GeS_2-Ga_2S_3$ system produces mobile complex anions of $MGaS_{3/2}Cl$, resulting in glass formation.[41] Further, increasing the CsI contents in $GeS_2-In_2S_3$ tends to decrease the glass transition temperature[42] and even the formability of glasses with a softening point below room temperature has been demonstrated in the GaI−NaCl system.[41] Various metal halides have also been introduced in chalcohalide or fluoride glasses to improve


https://doi.org/10.1021/acsenergylett.1c00545
ACS Energy Lett. 2021, 6, 2006−2015

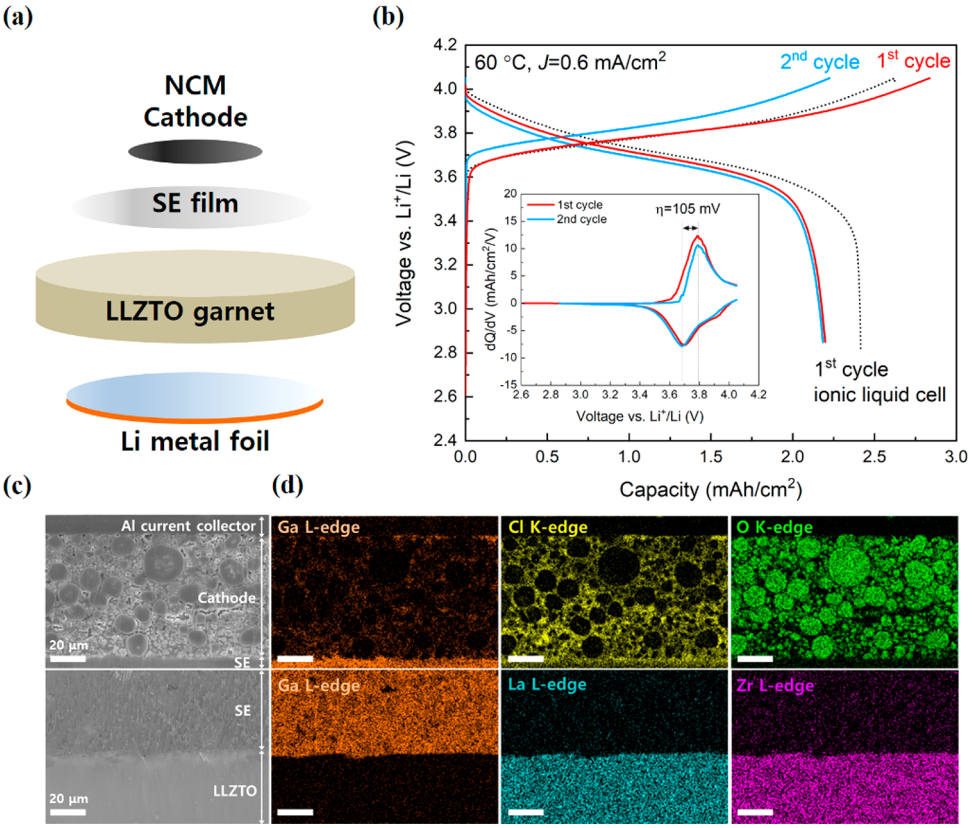


**Figure 3. Application of the 3LiCl−$GaF_3$ electrolyte in an ASSB. (a) Schematic figure of the cell configuration of the ASSB. (b) Voltage profile with a current density of 0.6 mA $cm^{-2}$ at 60 °C in the voltage range of 2.85−4.05 V. Inset: d$q$ d$V^{-1}$ curves of the first and second cycles. Dotted lines indicates the voltage profile with a Li/garnet/ionic liquid/cathode cell. (c) SEM and (d) EDS mapping images of an all-solid-state cell composed of a Li/LLZTO/3LiCl−$GaF_3$/cathode.**

glass-forming ability and lower the glass transition temperature by forming complex anions.[43,44]

Gallium-containing mobile complex anions of Ga−F−X (X: different halogens) are thus expected to induce viscoelasticity. In addition, compositions that form a clay-like solid show higher ionic conductivity than those remaining in the powder state. Amorphous or glass-type materials offer more room for improvement than their crystalline counterparts, because they can tolerate a wider range of changes in their chemical compositions. Adding a metal chloride as a dopant was feasible while maintaining a high ionic conductivity over 1 mS $cm^{-1}$ (Table 1). Thus, the properties of the clay-like solid electrolytes, such as their ionic conductivity, mechanical properties, electrochemical stability window, and chemical reactivity toward the cathode can be more easily tailored by tuning and optimizing the complex anion composition.

*Application in all-solid-state batteries and degradation mechanism.* The $x$LiCl−$GaF_3$ solid electrolyte has an intrinsically vulnerable electrochemical stability against the Li metal anode for ASSBs; thus, it was demonstrated as a catholyte. The assembled ASSBs consisted of LLZTO, which is stable against Li metal, and the $x$LiCl−$GaF_3$ electrolyte covered by a commercial cathode cast on an Al current collector (NCM111 with 96 wt %), which is usually used in conventional lithium-ion batteries. Solid-state batteries were assembled with a configuration of Li/LLZTO/SE film/NCM111 cathode by applying a cold isostatic pressure of 250 MPa for 3 min (Figure 3(a)).

A galvanostatic charge−discharge test was performed on the assembled cell at 60 °C with a current density of 0.6 mA $cm^{-2}$ using 3LiCl−$GaF_3$ in the voltage range of 2.85−4.05 V vs $Li^+$/Li (Figure 3(b)) given its superior chemical stability compared to that of $x$ = 2, as shown in Figure S13. The ability to employ thick electrodes with high loading densities has the potential to dramatically increase the volumetric energy density of ASSBs thanks to the large areal capacity, whereas most reported, garnet-based, solid-state batteries usually deliver 0.2−1.5 mAh $cm^{-2}$.[45] The first charge capacity was 2.84 mAh $cm^{-2}$ (i.e., 160 mAh $g^{-1}$), which is a comparable value to that of an ionic liquid electrolyte cell in the same voltage range (2.62 mAh $cm^{-2}$) (Figure 3(b)). Similar results were observed at 25 °C (Figure S14), which implies that the 3LiCl−$GaF_3$ solid electrolyte is feasible as catholyte not only at 60 °C but also at room-temperature operation. Given the fact that liquid electrolytes can form perfect interfaces with cathodes, the comparable first charge capacity of ASSBs implies a homogeneous distribution of the solid electrolyte in the porous cathode that can form well-defined ionic conduction paths. Thus, all cathode particles can participate in the electrochemical reaction, even in a thick electrode with a high loading density (~20 mg $cm^{-2}$). Interestingly, the solid electrolyte fills the porous region of a cathode with 70 $\mu$m thickness (Figure 3(c)), as confirmed by the Ga and Cl signals from energy-dispersive spectroscopy (EDS) mapping (Figure 3(d)), which implies that the viscoelastic solid electrolyte can provide intimate contact not


https://doi.org/10.1021/acsenergylett.1c00545
ACS Energy Lett. 2021, 6, 2006−2015

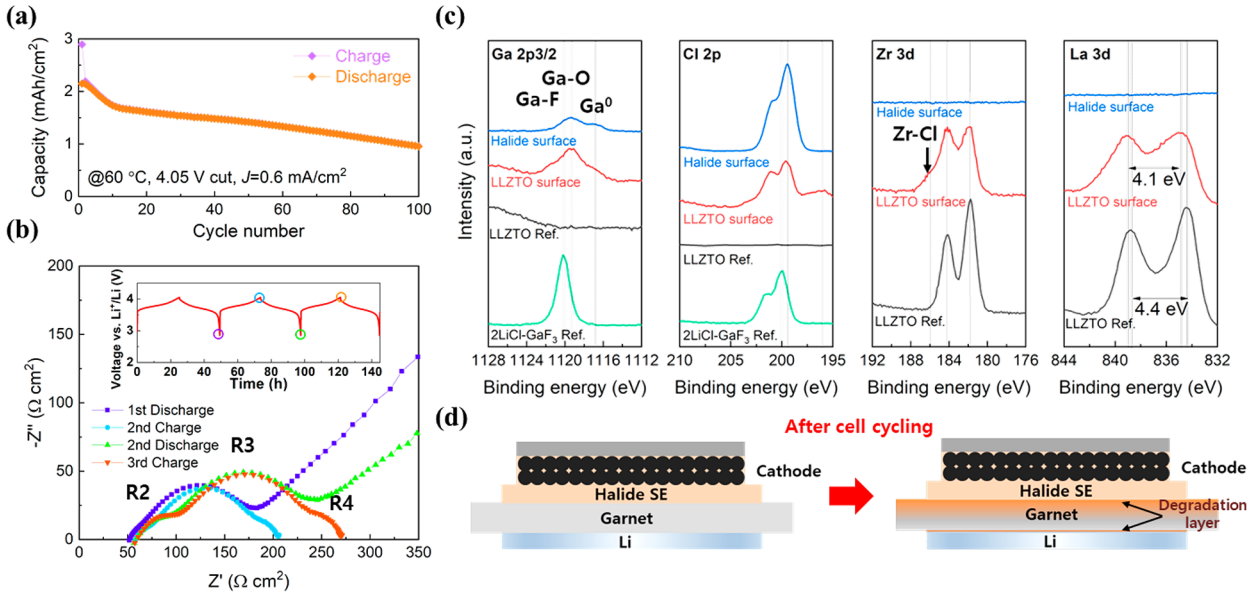


**Figure 4. Cycle life and cell degradation. (a) Cycle life of an all-solid-state cell with a current density of 0.6 mA cm$^{-2}$ at 60 °C. (b) Electrochemical impedance spectra after charge and discharge. Inset: voltage profile at a current density of 0.1 mA cm$^{-2}$ and 60 °C. (c) XPS of the garnet/halide solid electrolyte interface after cell degradation. Red and blue indicate the surface of garnet and halide solid electrolyte, respectively. (d) Schematic figure of the degradation mechanism of Li/garnet/3LiCl−$GaF_3$/NCM cathode solid-state batteries.**

only with LLZTO garnet but also with the porous cathode electrode.

Beyond its feasibility, to successfully employ the pliable electrolyte in ASSBs, its remaining issues of a narrow electrochemical stability window and chemical reactivity must be resolved. High-voltage operation is inevitable for high-energy-density systems; however, the solid electrolyte showed a parasitic reaction above 4.1 V in both the galvanostatic charge profile and the d$q$ d$V^{-1}$ analysis in the voltage range of 2.85−4.2 V (Figure S15). Additionally, the first discharge of 2.15 mAh cm$^{-2}$ showed a low Coulombic efficiency of approximately 74.2% (Figure 3(b)), which implies the occurrence of side reactions in solid electrolyte. Specifically, as shown in Figure 4(a), only 45% of the capacity was retained after 100 cycles at 60 °C. This degradation was induced by the increasing interfacial resistance during cycling. The cathode−SE interfacial resistance increased more during discharge than during charge, which is similar to the increasing resistance observed in $LiCoO_2$−In cells with $Li_{10}GeP_2S_{12}$ caused by a chemical reaction during cycling.[23] As shown in Figure 4(b), two semicircles are observed regardless of the state of charge, which correspond to the resistances of the garnet−SE (R2) and cathode−SE (R3) interfaces according to capacitance value from EIS fitting (Table S3) with an equivalent circuit shown in Figure S16. Resistance from the semicircle in the low-frequency region (R4) is considered to be originated by an electrochemical reaction including a charge transfer reaction at the cathode−SE interface, given that the capacitance value is in the range of $10^{-5}$∼$10^{-4}$ F.[46] Both R2 and R3 increased more during discharge than during the charge process, and the proportion of R2 to the total resistance rapidly increased with the number of cycles (Figures S16−S18), indicating more severe degradation of the garnet−SE interface. According to the results in EIS fitting, the capacitance value of C3 (parallel connected to R3, $10^{-8}$∼$10^{-7}$ F) and corresponding to SE/cathode interface were maintained during cycling; however, the value of C2 (parallel connected to R2, $10^{-9}$∼$10^{-8}$ F) corresponding to garnet/SE interface decreased as the cycle number. It is analogous to the capacitance decrease phenomenon usually observed at the interface where a chemical reaction occurs (e.g., argyrodite $Li_6PS_5Cl$/bare NCM cathode interface).[4] It implies a chemical reaction or formation of an interfacial layer such as a solid electrolyte interphase (SEI) at the garnet−SE interface. After cell disassembly, the chemical diffusion of Ga and Cl into the garnet was confirmed by EDS mapping images (Figure S19). Chemical diffusion at the interface induced not only reduction of Ga ions but also the formation of Zr−Cl bonds and LaOCl, as confirmed by the XPS results (Figure 4(c)). Both garnet and the solid electrolyte surface showed lower energy shifts in the binding energy from 1120.3 to 1119.3 eV and new peak emergence at 1116.8 eV, which indicates the Ga−O bond formation and reduction of the Ga ion.[47] The intensity increase at 184.0 and 186.0 eV in the Zr 3d region is similar to peaks observed for $ZrCl_4$, and the decrease of the Cl binding energy from 200.0 to 199.4 eV supports the formation of metal chloride.[48] When combined, the change in Cl 2p and the decrease of the La $3d_{5/2}$ doublet splitting energy from 4.4 to 4.1 eV implies the formation of LaOCl, given that the magnitude of the multiplet splitting is sensitive to the ligand atoms.[49] The observed peak of La 4p at 196.0 eV and postmortem analysis also support the formation of LaOCl, which has $Cl^-$ ion conductivity,[50] because $Cl^-$ ions were detected from the Li metal surface after cell degradation (Figure S20). These observations were further corroborated by DFT calculations, which predicted the formation of several compounds, including LaClO, $LiGaO_2$, and LiCl at the interface between 3LiCl−$GaF_3$ and LLZTO with a high reaction energy of 137 meV/atom (Figure S21(a)). This chemical degradation was found to be worse in the high-voltage region within a battery operating voltage window (2−4.5 V), as the reaction energy between 3LiCl−$GaF_3$ and LLZTO further increased to above 200 meV/atom over 4 V


https://doi.org/10.1021/acsenergylett.1c00545
ACS Energy Lett. 2021, 6, 2006−2015

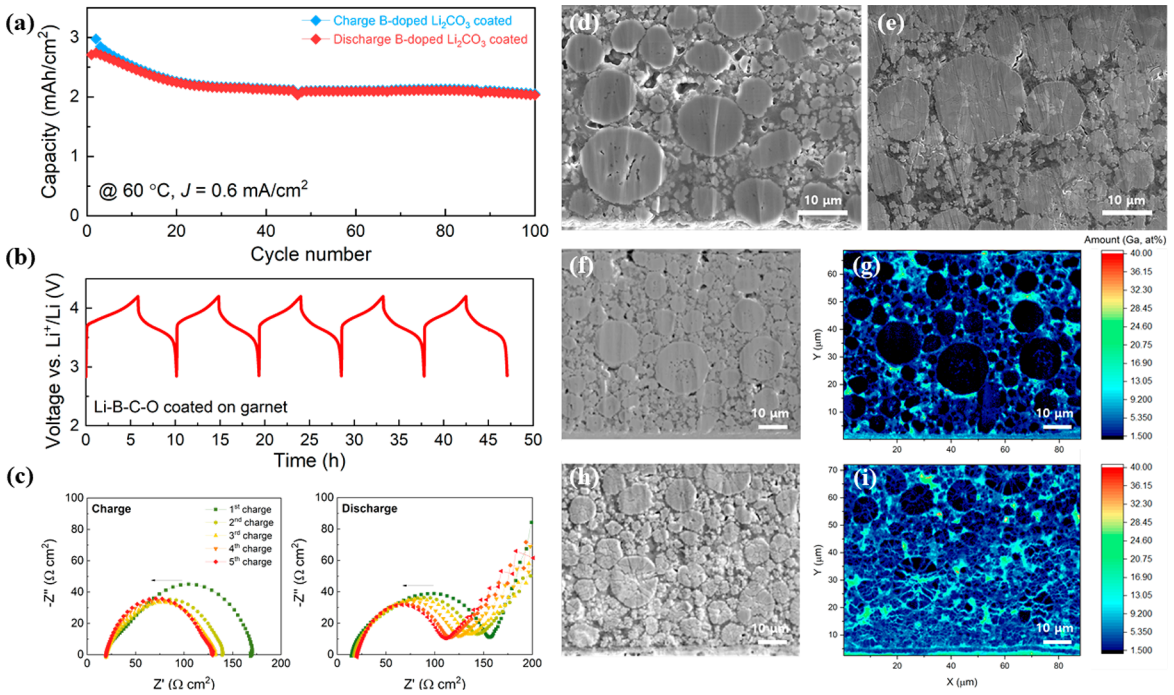


**Figure 5. Improved cycle life by mitigation of the chemical reaction with garnet and preservation of the physical contact with the cathode. (a) Cycle life of an all-solid-state cell including a Li−B−C−O interlayer between 3LiCl−$GaF_3$ and garnet with a current density of 0.6 mA $cm^{-2}$ at 60 °C. (b) Voltage profile at a current density of 0.6 mA $cm^{-2}$ and 60 °C for in situ EIS analysis after charging and discharging. (c) EIS spectra after charging and discharging during the initial five cycles. Cross-sectional SEM images of the cathode with a 3LiCl−$GaF_3$ solid electrolyte for the (d) fresh cell and (e) cell after 50 cycles. SEM images and electron probe microanalysis (EPMA) mappings of gallium in (f,g) the fresh cell and (h,i) cell after 50 cycles, respectively.**

(Figure S21(b) and Table S4). The overall degradation mechanism is schematically shown in Figure 4(d). The chemical degradation layer was observed in both interfaces of the garnet/solid electrolyte and garnet/Li forming Zr−Cl, Ga−O, LaOCl, and LiCl, respectively, due to the chemical reaction. This chemical reaction induced the decrease of the bulk ionic conductivity of garnet from 0.74 to 0.34 mS $cm^{-1}$.

*Mitigation of the chemical reaction and improved cyclability.* To mitigate the undesirable chemical reaction between xLiCl−$GaF_3$ and garnet, we introduced an interlayer that was chemically stable to both components. The interlayer material was hierarchically searched through high-throughput calculations of interface reaction energies (See methods for details). Among the candidate materials, we selected B-doped $Li_2CO_3$, which is well-known as a coating material with good lithium ionic conductivity.[51] DFT calculations revealed that B-doped $Li_2CO_3$ could effectively suppress the interfacial degradation between xLiCl−$GaF_3$ and garnet. As discussed in the previous section, the reaction energy of the original 3LiCl−$GaF_3$/garnet interface is 137 meV/atom. However, the introduction of a B-doped $Li_2CO_3$ protection layer between two electrolyte layers was found to produce less reactive interfaces, as described in Figure S22 and Table S5. We also discovered that the stabilization effect was more pronounced as carbon composition increased in $Li_{2+x}C_{1-x}B_xO_3$. Based on these predictions, B-doped $Li_2CO_3$ was applied on the garnet surface through heat treatment after spin coating the solution of LiOH and $H_3BO_3$ with a carboxymethyl cellulose (CMC) binder (Figure S23). Given that the structure of interlayer was similar to that of $Li_2CO_3$ (Figure S23(c)), not $Li_3BO_3$, the amount of boron was expected to be less than $x = 0.5$ in $Li_{2+x}C_{1-x}B_xO_3$.[51] The thickness of the interlayer was confirmed as 1−3 $\mu$m through the cross-sectional SEM image and EDS analysis (Figure S24). After an interlayer was applied, more than 80% of the initial capacity was retained after 100 cycles, as shown in Figure 5(a), and the interfacial resistance of the semicircles was slightly decreased during charging and discharging, as shown in Figure 5(b,c). These results were in stark contrast to the progressive electrochemical degradation shown in Figure 4(a,b). For detailed analysis, we applied the distribution of relaxation time (DRT) analysis to interpret EIS change as cycles.[52] In DRT results of a charged cell in Figure 5(c) (Figure S25), unresolved semicircles (R2, R3, and R4) were separated by the time constant. In contrast to the Li/garnet/3LiCl−$GaF_3$/NCM cell (Figure S25(a)), a Li−B−C−O interlayer applied cell showed a decrease in intensity of both R2 (38 000 Hz) and R3 (650 Hz) peaks (Figure S25(b)). It indicates that chemical reaction at the garnet/3LiCl−$GaF_3$ interface is mitigated by Li−B−C−O interlayer, and even further, it is effective to the mitigation of chemical degradation at the 3LiCl−$GaF_3$/NCM interface as denoted as R3. Comparative DRT analysis implies that chemical reaction between garnet and 3LiCl−$GaF_3$ could lead to bulk degradation of SE that can induce the sluggish charge transfer kinetics to the NCM cathode. The improved capacity retention was due to the mitigation of chemical diffusion of Cl and Ga ions to garnet, which was confirmed by SEM and EDS analysis after battery cycling (Figure S26). These results confirmed that the introduction of B-doped $Li_2CO_3$ effectively suppressed the chemical reaction between 3LiCl−$GaF_3$ and garnet, which was the main reason for cycle degradation.

The viscoelastic characteristics of the 3LiCl−$GaF_3$ solid electrolyte also contributed to its stable cycling performance by maintaining the physical contact with the NCM cathode


https://doi.org/10.1021/acsenergylett.1c00545
ACS Energy Lett. 2021, 6, 2006−2015

particles during battery cycling. As shown in Figure 5(d,e), the FIB-SEM images before and after battery cycling indicated that intimate contact between 3LiCl−$GaF_3$ and the cathode was well-maintained even after battery cycling, due to the similarities to the original state of the fresh cell, aside from crack formation in the secondary cathode particles. The Ga signal from the solid electrolyte was detected in the EPMA analysis even in the grain boundaries of the primary cathode particles after cycling (Figure 5(f−i)), which indicated that 3LiCl−$GaF_3$ could smear into voids or cracked regions that were formed due to the stress induced by the volumetric change of the cathode particles. In contrast to the sulfide-based solid electrolyte that showed physical contact loss during battery cycling, even under pressure, this clay-like property enabled the maintenance of physical contact with the cathode particles without the external pressure.

The mitigation of the chemical reaction and interfacial evolution between 3LiCl−$GaF_3$ and the interlayer or cathode is schematically shown in Figure S27. At the 3LiCl−$GaF_3$/interlayer interface, the B-doped $Li_2CO_3$ interlayer effectively blocked the diffusion of Cl and Ga ions to garnet and stabilized the interface by forming thermodynamically stable compounds, suspected to be the Cl-rich phase due to the brighter signal of Cl in the EDS analysis from the interlayer compared to the signal from 3LiCl−$GaF_3$ (Figure S26). At the 3LiCl−$GaF_3$/NCM cathode interface, although physical contact was well-maintained even after battery cycling, the slight initial cycle degradation implied the occurrence of the chemical reaction.

In the present work, a new type of solid electrolyte that demonstrated both high ionic conductivity (3.6 mS $cm^{-1}$) and gum-like viscoelasticity (complex shear moduli = 0.2 MPa) was discovered. The unique, viscoelastic, "glassy" property was believed to be due to the formation of gallium-containing, mobile, complex anions of Ga−F−X (X: different halogens); solid electrolytes showing viscoelastic behavior tend to exhibit high ionic conductivity (Table 1). In this context, the effect of different halogen atoms can be further investigated in terms of ionic conductivity and conduction mechanism. Since the solid electrolyte was vulnerable to reduction stability due to the reduction of Ga, it was used as the catholyte to solve the inhomogeneous point contact problem between the cathode and solid electrolyte. Due to its pliable characteristics, it was beneficial for forming and maintaining intimate contact with the cathode active material, even in commercialized, porous, and thick electrodes during battery cycling. Garnet was used as the anolyte by forming a garnet/$x$LiCl−$GaF_3$ interface; however, chemical diffusion of Cl and Ga to garnet degraded the cycling performance of the all-solid-state battery. This chemical reaction between the catholyte and anolyte was mitigated by coating the garnet surface using B-doped $Li_2CO_3$, which was chemically stable with both garnet and the $x$LiCl−$GaF_3$ solid electrolyte, forming a stable interlayer between the garnet and the $x$LiCl−$GaF_3$; as a result, a stable cycling performance was achieved. These results implied that, given the vulnerable cathodic stability of halide solid electrolytes,[53] halide solid electrolytes must be used as catholytes in combination with other solid electrolytes that are stable to lithium metal to use Li metal in high-energy-density, solid-state batteries. This indicated that the chemical reaction between halide and the other solid electrolyte could be a potential issue for the use of halide solid electrolytes. As shown in Figure S28, 3LiCl−$GaF_3$ showed chemical reactivity with a sulfide-based argyrodite solid electrolyte, which means that $x$LiCl−$GaF_3$ is not compatible with argyrodite. After 2 days of aging even at 25 °C, the total resistance increased to a value of 15 times higher than that of fresh cells. The chemical reactivity of $x$LiCl−$GaF_3$, not only with other solid electrolytes, including garnet, but also with the cathode active particles should be further investigated. In addition, regarding the reactivity of $x$LiCl−$GaF_3$ with its counterparts in forming an interface, the ion conduction behavior of Ga, Cl, and F in $x$LiCl−$GaF_3$ must be studied, where the chemical diffusivity of each ion could be controlled or mitigated using either a cation-mixing or anion-mixing effect through cation or anion doping.[44] Given a potential, wide range of chemical compositions in amorphous or glass-type materials that can be tolerated, as confirmed in Table 1, various solid electrolytes can be designed. Therefore, the discovery of a new class of solid electrolytes with high ionic conductivity and pliability can be not only an alternative solution to the problematic solid−solid contact issue with solid electrolytes and cathodes but also a framework for designing new solid electrolytes for the development of high-energy-density ASSBs.

## ■ ASSOCIATED CONTENT

### Supporting Information

The Supporting Information is available free of charge at https://pubs.acs.org/doi/10.1021/acsenergylett.1c00545.

Materials and methods; Figures S1−S28; Tables S1−S5 (PDF)

Video S1. Shape transformation of pliable electrolyte by kneading (MP4)

## ■ AUTHOR INFORMATION


### Corresponding Authors

**Sung-Kyun Jung** − *Next Generation Battery Lab, Material Research Center, Samsung Advanced Institute of Technology (SAIT), Samsung Electronics Co., Ltd., Suwon-si, Gyeonggi-do 16678, Republic of Korea;* orcid.org/0000-0002-3708-3757; Email: sk0726.jung@samsung.com

**Hyeokjo Gwon** − *Next Generation Battery Lab, Material Research Center, Samsung Advanced Institute of Technology (SAIT), Samsung Electronics Co., Ltd., Suwon-si, Gyeonggi-do 16678, Republic of Korea*; Email: h.gwon@samsung.com

### Authors

**Gabin Yoon** − *Next Generation Battery Lab, Material Research Center, Samsung Advanced Institute of Technology (SAIT), Samsung Electronics Co., Ltd., Suwon-si, Gyeonggi-do 16678, Republic of Korea*

**Lincoln J. Miara** − *Advanced Materials Lab, Samsung Research America, Cambridge, Massachusetts 02138, United States*

**Valentina Lacivita** − *Advanced Materials Lab, Samsung Research America, Cambridge, Massachusetts 02138, United States*

**Ju-Sik Kim** − *Next Generation Battery Lab, Material Research Center, Samsung Advanced Institute of Technology (SAIT), Samsung Electronics Co., Ltd., Suwon-si, Gyeonggi-do 16678, Republic of Korea*

Complete contact information is available at: https://pubs.acs.org/10.1021/acsenergylett.1c00545

### Author Contributions

[§]S.-K.J and H.G. contributed equally to this work.

### Author Contributions

S.-K.J and H.G. conceived and designed the overall experiments, performed experiments, analyzed the data, and wrote the manuscript. G.Y. assisted the material design and performed DFT calculations on the reduction stability of the electrolyte and designed the interlayer. L.J.M. and V.L. assisted the interlayer design, and J.-S.K. contributed to the full-cell battery experiments. All the authors participated in discussion and provided constructive advice for experimental design.

### Notes

The authors declare no competing financial interest.

## ■ ACKNOWLEDGMENTS

This work was supported by funds from Samsung Electronics Co. Ltd.

## ■ REFERENCES

(1) Zhang, Z.; et al. New horizons for inorganic solid state ion conductors. *Energy Environ. Sci.* **2018**, *11*, 1945−1976.
(2) Randau, S.; et al. Benchmarking the performance of all-solid-state lithium batteries. *Nature Energy* **2020**, *5*, 259−270.
(3) Xiao, Y.; et al. Understanding interface stability in solid-state batteries. *Nature Reviews Materials* **2020**, *5*, 105−126.
(4) Jung, S.-K.; et al. Understanding the effects of chemical reactions at the cathode−electrolyte interface in sulfide based all-solid-state batteries. *J. Mater. Chem. A* **2019**, *7*, 22967−22976.
(5) Koerver, R.; et al. Capacity Fade in Solid-State Batteries: Interphase Formation and Chemomechanical Processes in Nickel-Rich Layered Oxide Cathodes and Lithium Thiophosphate Solid Electrolytes. *Chem. Mater.* **2017**, *29*, 5574−5582.
(6) Krauskopf, T.; Hartmann, H.; Zeier, W. G.; Janek, J. Toward a Fundamental Understanding of the Lithium Metal Anode in Solid-State Batteries—An Electrochemo-Mechanical Study on the Garnet-Type Solid Electrolyte $Li_{6.25}Al_{0.25}La_3Zr_2O_{12}$. *ACS Appl. Mater. Interfaces* **2019**, *11*, 14463−14477.
(7) Krauskopf, T.; Mogwitz, B.; Rosenbach, C.; Zeier, W. G.; Janek, J. Diffusion Limitation of Lithium Metal and Li−Mg Alloy Anodes on LLZO Type Solid Electrolytes as a Function of Temperature and Pressure. *Adv. Energy Mater.* **2019**, *9*, 1902568.
(8) Kim, S.; et al. The Role of Interlayer Chemistry in Li-Metal Growth through a Garnet-Type Solid Electrolyte. *Adv. Energy Mater.* **2020**, *10*, 1903993.
(9) Murugan, R.; Thangadurai, V.; Weppner, W. Fast Lithium Ion Conduction in Garnet-Type $Li_7La_3Zr_2O_{12}$. *Angew. Chem., Int. Ed.* **2007**, *46*, 7778−7781.
(10) Kamaya, N.; et al. A lithium superionic conductor. *Nat. Mater.* **2011**, *10*, 682−686.
(11) Asano, T.; et al. Solid Halide Electrolytes with High Lithium-Ion Conductivity for Application in 4 V Class Bulk-Type All-Solid-State Batteries. *Adv. Mater.* **2018**, *30*, 1803075.
(12) Kim, S.; et al. A complex hydride lithium superionic conductor for high-energy-density all-solid-state lithium metal batteries. *Nat. Commun.* **2019**, *10*, 1081.
(13) Baek, S.-W.; Lee, J.-M.; Kim, T. Y.; Song, M.-S.; Park, Y. Garnet related lithium ion conductor processed by spark plasma sintering for all solid state batteries. *J. Power Sources* **2014**, *249*, 197−206.
(14) Han, F.; et al. Interphase Engineering Enabled All-Ceramic Lithium Battery. *Joule* **2018**, *2*, 497−508.
(15) van den Broek, J.; Rupp, J. L. M.; Afyon, S. Boosting the electrochemical performance of Li-garnet based all-solid-state batteries with $Li_4Ti_5O_{12}$ electrode: Routes to cheap and large scale ceramic processing. *J. Electroceram.* **2017**, *38*, 182−188.
(16) Li, Y.; et al. Garnet Electrolyte with an Ultralow Interfacial Resistance for Li-Metal Batteries. *J. Am. Chem. Soc.* **2018**, *140*, 6448−6455.
(17) Zhang, N.; et al. Mechanism Study on the Interfacial Stability of a Lithium Garnet-Type Oxide Electrolyte against Cathode Materials. *ACS Applied Energy Materials* **2018**, *1*, 5968−5976.
(18) Miara, L.; et al. About the Compatibility between High Voltage Spinel Cathode Materials and Solid Oxide Electrolytes as a Function of Temperature. *ACS Appl. Mater. Interfaces* **2016**, *8*, 26842−26850.
(19) Janek, J.; Zeier, W. G. A solid future for battery development. *Nature Energy* **2016**, *1*, 16141.
(20) Yang, Y.; et al. Ionic liquid enhanced composite solid electrolyte for high-temperature/long-life/dendrite-free lithium metal batteries. *J. Membr. Sci.* **2020**, *612*, 118424.
(21) Yang, G.; Song, Y.; Wang, Q.; Zhang, L.; Deng, L. Review of ionic liquids containing, polymer/inorganic hybrid electrolytes for lithium metal batteries. *Mater. Des.* **2020**, *190*, 108563.
(22) Yang, X.; et al. High-areal-capacity all-solid-state lithium batteries enabled by rational design of fast ion transport channels in vertically-aligned composite polymer electrodes. *Nano Energy* **2019**, *61*, 567−575.
(23) Li, X.; et al. Air-stable $Li_3InCl_6$ electrolyte with high voltage compatibility for all-solid-state batteries. *Energy Environ. Sci.* **2019**, *12*, 2665−2671.
(24) Liang, J.; et al. Site-Occupation-Tuned Superionic $Li_xScCl_{3+x}$ Halide Solid Electrolytes for All-Solid-State Batteries. *J. Am. Chem. Soc.* **2020**, *142*, 7012−7022.
(25) Park, K.-H.; et al. High-Voltage Superionic Halide Solid Electrolytes for All-Solid-State Li-Ion Batteries. *ACS Energy Letters* **2020**, *5*, 533−539.
(26) Schlem, R.; et al. Mechanochemical synthesis: a tool to tune cation site disorder and ionic transport properties of $Li_3MCl_6$ (M= Y, Er) superionic conductors. *Adv. Energy Mater.* **2020**, *10*, 1903719.
(27) Schlem, R.; et al. Lattice Dynamical Approach for Finding the Lithium Superionic Conductor $Li_3ErI_6$. *ACS Applied Energy Materials* **2020**, *3*, 3684−3691.
(28) Youngman, R. NMR spectroscopy in glass science: a review of the elements. *Materials* **2018**, *11*, 476.
(29) Areán, C. O.; Delgado, M. R.; Montouillout, V.; Massiot, D. Synthesis and Characterization of Spinel-Type Gallia-Alumina Solid Solutions. *Z. Anorg. Allg. Chem.* **2005**, *631*, 2121−2126.
(30) Sakuda, A.; Hayashi, A.; Tatsumisago, M. Sulfide Solid Electrolyte with Favorable Mechanical Property for All-Solid-State Lithium Battery. *Sci. Rep.* **2013**, *3*, 2261.
(31) Mackanic, D. G.; et al. Decoupling of mechanical properties and ionic conductivity in supramolecular lithium ion conductors. *Nat. Commun.* **2019**, *10*, 5384.
(32) Braga, M. H.; Ferreira, J. A.; Stockhausen, V.; Oliveira, J. E.; El-Azab, A. Novel $Li_3ClO$ based glasses with superionic properties for lithium batteries. *J. Mater. Chem. A* **2014**, *2*, 5470−5480.
(33) Braga, M. H.; Murchison, A. J.; Ferreira, J. A.; Singh, P.; Goodenough, J. B. Glass-amorphous alkali-ion solid electrolytes and their performance in symmetrical cells. *Energy Environ. Sci.* **2016**, *9*, 948−954.
(34) Wang, Y.; Gozen, A.; Chen, L.; Zhong, W.-H. Gum-Like Nanocomposites as Conformable, Conductive, and Adhesive Electrode Matrix for Energy Storage Devices. *Adv. Energy Mater.* **2017**, *7*, 1601767.
(35) Kawamura, J.; Asayama, R.; Kuwata, N.; Kamishima, O. Ionic transport in glass and polymer: Hierarchical structure and dynamics. *Phys. Solid State Ionics* **2006**, *81*, 193−246.
(36) Schwietert, T. K.; et al. Clarifying the relationship between redox activity and electrochemical stability in solid electrolytes. *Nat. Mater.* **2020**, *19*, 428−435.
(37) Richards, W. D.; Miara, L. J.; Wang, Y.; Kim, J. C.; Ceder, G. Interface Stability in Solid-State Batteries. *Chem. Mater.* **2016**, *28*, 266−273.


https://doi.org/10.1021/acsenergylett.1c00545
*ACS Energy Lett.* 2021, 6, 2006−2015

(38) Hanghofer, I.; et al. Untangling the Structure and Dynamics of Lithium-Rich Anti-Perovskites Envisaged as Solid Electrolytes for Batteries. *Chem. Mater.* **2018**, *30*, 8134−8144.
(39) Liu, Y.; Cai, Z.; Tan, L.; Li, L. Ion exchange membranes as electrolyte for high performance Li-ion batteries. *Energy Environ. Sci.* **2012**, *5*, 9007−9013.
(40) Yim, C.-H.; Abu-Lebdeh, Y. A. Connection between phase diagram, structure and ion transport in liquid, aqueous electrolyte solutions of Lithium chloride. *J. Electrochem. Soc.* **2018**, *165*, A547.
(41) Tver'yanovich, Y. S.; Aleksandrov, V. V.; Murin, I. V.; Nedoshovenko, E. G. Glass-forming ability and cationic transport in gallium containing chalcohalide glasses. *J. Non-Cryst. Solids* **1999**, *256*−*257*, 237−241.
(42) Zhang, X.-H.; Adam, J.-L.; Bureau, B. Chalcogenide Glasses. *Springer Handbook of Glass* **2019**, 525−552.
(43) Tver'yanovich, Y. S.; Vlček, M.; Tverjanovich, A. Formation of complex structural units and structure of some chalco-halide glasses. *J. Non-Cryst. Solids* **2004**, *333*, 85−89.
(44) Tatsumisago, M.; Akamatsu, Y.; Minami, T. Ionic conductivity of $ZrF_4$-$BaF_2$-MX (M = Li, Na ; X = F, Cl) glasses. *Solid State Ionics* **1988**, *31*, 41−47.
(45) Tsai, C.-L.; et al. A garnet structure-based all-solid-state Li battery without interface modification: resolving incompatibility issues on positive electrodes. *Sustainable Energy & Fuels* **2019**, *3*, 280−291.
(46) Irvine, J. T.; Sinclair, D. C.; West, A. R. Electroceramics: characterization by impedance spectroscopy. *Adv. Mater.* **1990**, *2*, 132−138.
(47) Muscat, A. J. (Invited) Reaction Mechanisms on Binary III-V Semiconductor Surfaces during Etching, Passivation, and Deposition. *ECS Trans.* **2015**, *69*, 217−226.
(48) Roy, P. C.; Jeong, H. S.; Doh, W. H.; Kim, C. M. Atomic Layer Deposition (ALD) of $ZrO_2$ in Ultrahigh Vacuum (UHV). *Bull. Korean Chem. Soc.* **2013**, *34*, 1221.
(49) Li, J. P. H.; et al. Understanding of binding energy calibration in XPS of lanthanum oxide by in situ treatment. *Phys. Chem. Chem. Phys.* **2019**, *21*, 22351−22358.
(50) Nunotani, N.; et al. Structural environment of chloride ion-conducting solids based on lanthanum oxychloride. *J. Am. Ceram. Soc.* **2020**, *103*, 297−303.
(51) Jung, S. H.; et al. $Li_3BO_3$−$Li_2CO_3$: rationally designed buffering phase for sulfide all-solid-state Li-ion batteries. *Chem. Mater.* **2018**, *30*, 8190−8200.
(52) Wan, T. H.; Saccoccio, M.; Chen, C.; Ciucci, F. Influence of the discretization methods on the distribution of relaxation times deconvolution: implementing radial basis functions with DRTtools. *Electrochim. Acta* **2015**, *184*, 483−499.
(53) Riegger, L. M.; Schlem, R.; Sann, J.; Zeier, W. G.; Janek, J. Lithium-Metal Anode Instability of the Superionic Halide Solid Electrolytes and the Implications for Solid-State Batteries. *Angew. Chem., Int. Ed.* **2021**, *60*, 6718−6723.


https://doi.org/10.1021/acsenergylett.1c00545
*ACS Energy Lett.* 2021, 6, 2006−2015